

We are IntechOpen, the world's leading publisher of Open Access books Built by scientists, for scientists

4,800

Open access books available

122,000

International authors and editors

135M

Downloads

Our authors are among the

154

Countries delivered to

TOP 1%

most cited scientists

12.2%

Contributors from top 500 universities



WEB OF SCIENCE™

Selection of our books indexed in the Book Citation Index
in Web of Science™ Core Collection (BKCI)

Interested in publishing with us?
Contact book.department@intechopen.com

Numbers displayed above are based on latest data collected.

For more information visit www.intechopen.com



A Performance Review of 3D TOF Vision Systems in Comparison to Stereo Vision Systems

Stephan Hussmann¹, Thorsten Ringbeck² and Bianca Hagebecker²

¹Westcoast University of Applied Sciences

²PMDTechnologies GmbH
Germany

1. Introduction

The most common and well-known principle of 3D image acquisition is stereo vision (SV). This principle of 3D-image acquisition is already known and used for decades in the research community. The advantage of stereo vision to other range measuring devices such as laser scanners, acoustic or radar sensors is that it achieves high resolution and simultaneous acquisition of the entire range image without energy emission or moving parts.

Still, the major disadvantage is the limited Field of View (FOV) and the correspondence problem. To enhance the FOV many techniques are researched such as rotating cameras (Kang et al., 1997; Benosman et al., 1996; Krishnan et al., 1996), increasing the number of the cameras (Kawanishi et al., 1998), and the use of a special optic (Liancheng & Feng, 2005; Lin & Bajcsy, 2003). Also a combination of 1D-laser scanner and a SV system are proposed to overcome the FOV problem (Cheng et al., 2002). However, these systems are expensive and not easy to synchronize. Due to the correspondence problem algorithms need to be improved to give a lower percentage of false matches as well as better accuracy of depth estimates. Performance of algorithm needs to be evaluated over a broad range of image types in order to test their robustness (Dhond & Aggarwal, 1989).

In the past years the modality of Time-of-Flight (TOF) imaging became more and more attractive to a growing research community (Schwarte_a et al., 1997; Schwarte_b et al., 1997). Because of the enormous progress in TOF-vision systems, nowadays 3D matrix cameras can be manufactured and be used for many application such as robotic, automotive, industrial, medical and multimedia applications. Due to the increasing demand of safety requirements in the automotive industry it can be assumed that the TOF-camera market will grow and the unit price of these systems in the mass production will drop down to ca. 100 € (Hussmann & Hess, 2006).

For all application areas new accurate and fast algorithms for 3D object recognition and classification are needed. As now commercial 3D-TOF cameras are available at a reasonable price the number of research projects is expected to increase significantly. One early example of using a TOF-camera based on the Photonic-Mixer-Devices (PMD)-Technology for 3D object recognition in TOF data sets are presented in (Hess et al., 2003). In this paper the transition from a general model of the system to specific applications such as intelligent

Source: Stereo Vision, Book edited by: Dr. Asim Bhatti,
ISBN 978-953-7619-22-0, pp. 372, November 2008, I-Tech, Vienna, Austria

airbag control and robot assistance in surgery are demonstrated. A more current example in using a PMD-TOF camera on a robot system, highlighting the advantages of TOF- compared to SV-vision systems, is reported in (Husmann & Liepert, 2007).

This chapter is structured as follows. In Section II we expose the issues which motivate a new approach for 3D image acquisition systems. In Section III we derive the equation set needed to design a 3D TOF vision system. In Section IV automotive applications will demonstrate the usability of 3D-TOF vision systems based on the PMD-technology fulfilling the tough target settings in the automotive industry. Concluding remarks will summarize the paper.

2. Comparison of TOF- and SV vision systems

2.1 Working principle

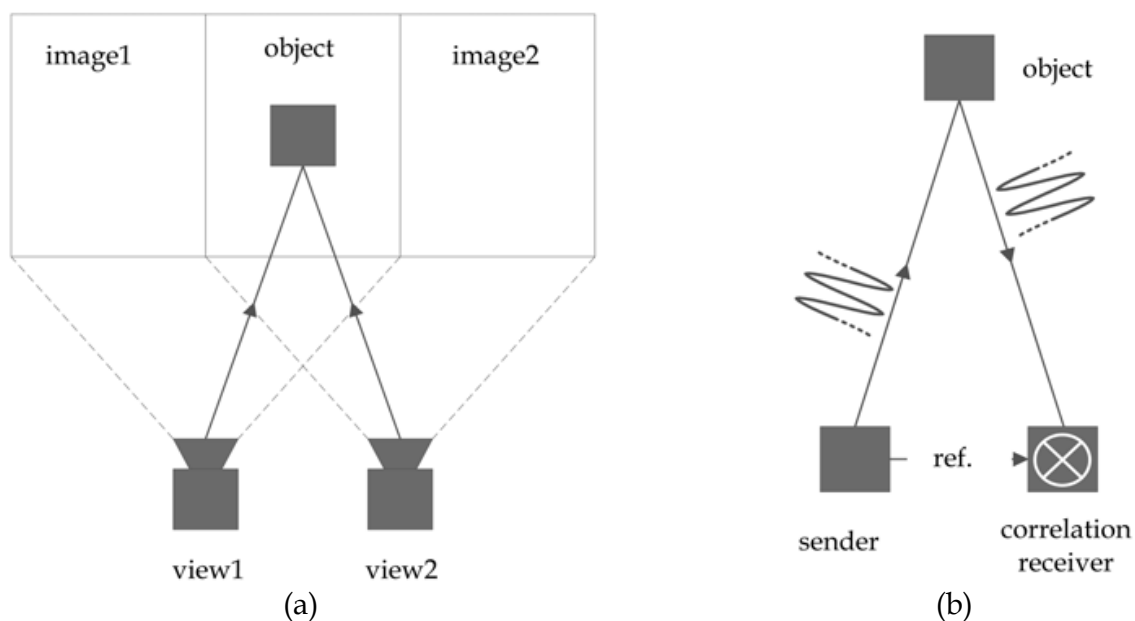


Fig. 1. Working principle of (a) SV vision systems and (b) TOF vision systems (Husmann & Hess, 2006)

Common stereo vision systems comprise two perspective cameras with limited FOV. As shown in Fig. 1 (a) a physical point is taken up in the observed 3D-space by two perspective cameras. If the corresponding pixel of this point is found in both camera images, the position can be computed with the help of the triangulation principle. The major problem is to detect the corresponding pixels as they are required to estimate the range information correctly (*correspondence problem*). High processing power and time can be consumed if those pixels cannot be found easily. Fig. 1 (b) shows the working principle of TOF vision systems. TOF is an active range system and needs an illumination source. The range information is measured by emitting a modulated near-infrared light signal and computing the phase of the received reflected light signal. Using the PMD-Technology the phase calculation is carried out in each individual pixel of the sensor matrix (Schwarte_a et al., 1997; Schwarte_b et al., 1997). Hence TOF offers a direct depth data acquisition, whereas SV involves a great amount of computational power for the same 3D image. However SV systems can be realized without active illumination.

2.2 Image processing chain

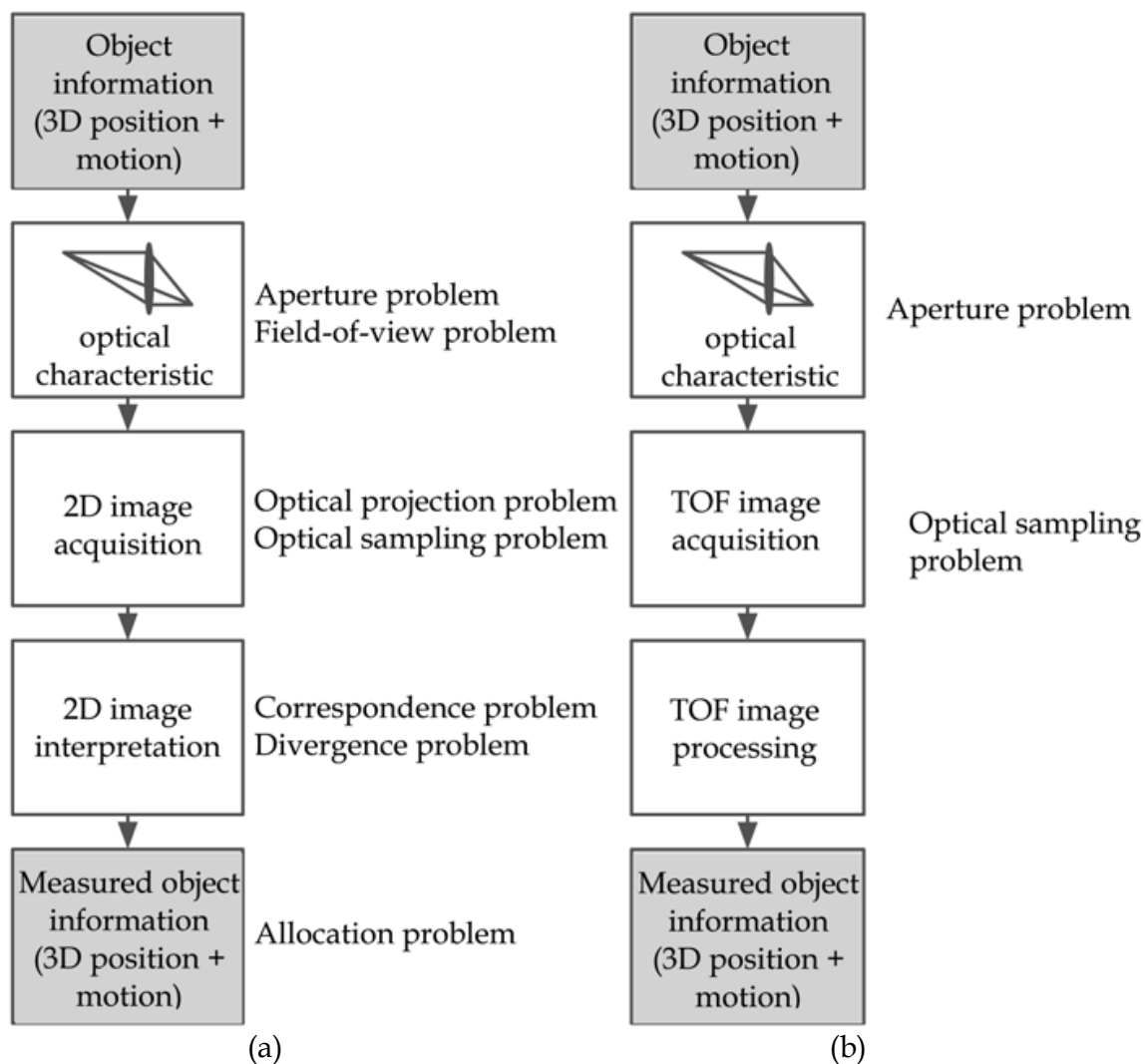


Fig. 2. Functional block diagram of the image processing chain of (a) SV vision systems and (b) TOF vision systems (Hussmann & Hess, 2006)

In Fig. 2 (a) the functional block diagram of the image processing chain of SV systems is shown. Several problems arise during the image processing of the captured object information. Due to the limited aperture angle of the camera optics only a certain part of the environment can be detected (*aperture problem*). The FOV is usually fixed for one application and cannot be changed easily (*FOV problem*). The optical projection of the objects on a planar sensor leads to a complete loss of the 3D-information (*optical projection problem*). Due to the sampling rate of the image sensor the detection of very fast objects is limited (*optical sampling problem*). The *correspondence problem* is already explained in the last section and will be described in more detail in the following section. A change in the gray level values of both cameras is not necessarily caused by an object movement. For example illumination changes could also cause gray level changes. Hence the object motion cannot be described by the gray level values changes (*divergence problem*). At last the *allocation problem* is stated. The estimated range values of the scene are not evenly distributed due to the correspondence problem.

TOF vision systems suffer fewer problems as shown in Fig. 2 (b). The *FOV problem* does not depend on the chosen hardware setup and can be changed by software easily. In the next section more details are provided. The object information is not lost by the optical projection of the objects on a planar sensor. Each pixel of the sensor calculates a range value. A reconstruction of range values based on gray level values does not exist. Hence no *correspondence*, *divergence* and *allocation problem* is given. Only the *aperture* and *sampling problem* still exists.

2.3 Field-of-view problem

The depth resolution of SV vision systems depends on the chosen optical arrangement of the two cameras which defines the triangle's angles. TOF systems do not depend on geometrical parameters. They are using an active modulated light source. Two modulation techniques are the most common one, pulsed modulation (Moring et al., 1989) or continuous wave (CW) modulation (Beheim & Fritsch, 1986). In the currently available TOF cameras CW-modulation is used as for this mode extremely high rise and fall times are not required and for this reason a larger variety of light sources are available. Mostly square waves are used, but other waveforms such as sinusoidal waves are suitable modulation signals. Using CW-modulation the phase difference between the sent and received optical signal is measured, rather than directly measuring a light pulse's turn-around time. As the modulation frequency f_{mod} is known, the measured phase φ_0 directly corresponds to the time of flight (Lange, 2000). Equation (1) describes how the range of TOF vision systems can be determined. The physical constant for the speed of light ($3 \cdot 10^8$ m/s) is given by c and N represents the ambiguity in range estimation.

$$R = \frac{c}{2 \cdot f_{mod}} \cdot \left(\frac{\varphi_0}{360^\circ} + N \cdot 360^\circ \right) \text{ with } N = 0, 1, 2, 3, \dots \quad (1)$$

A very common modulation frequency of TOF vision systems is $f_{mod} = 20$ MHz. This leads to a non-ambiguity range (NAR) of 7.5 m as derived in Equation (2). There are two reasons for choosing this modulation frequency. One reason is that no high-power IR-LEDs are available with a higher modulation frequency at a low price tag and the other reason is that the NAR suits most of the indoor and outdoor applications.

$$NAR = \frac{c}{2 \cdot f_{mod}} = \frac{3 \cdot 10^8}{2 \cdot 20 \cdot 10^6} = 7.5 \text{ m} \quad (2)$$

The FOV of TOF vision systems depend only on the modulation frequency as derived in Equation (1) and (2). A high modulation frequency leads to short measuring range and vice versa.

2.4 Correspondence problem

As mentioned before the correspondence problem is a major problem as the range values can only be estimated in image regions with adequate gray level value changes. As a consequence a SV vision system will always have difficulties acquiring 3D information of objects with equal gray level values such as walls, roadways and so forth. Also objects with the same gray level value at different distances are difficult to distinguish. These problems

can be compensated with advanced SV algorithms using a lot of processing power compared to TOF vision systems.

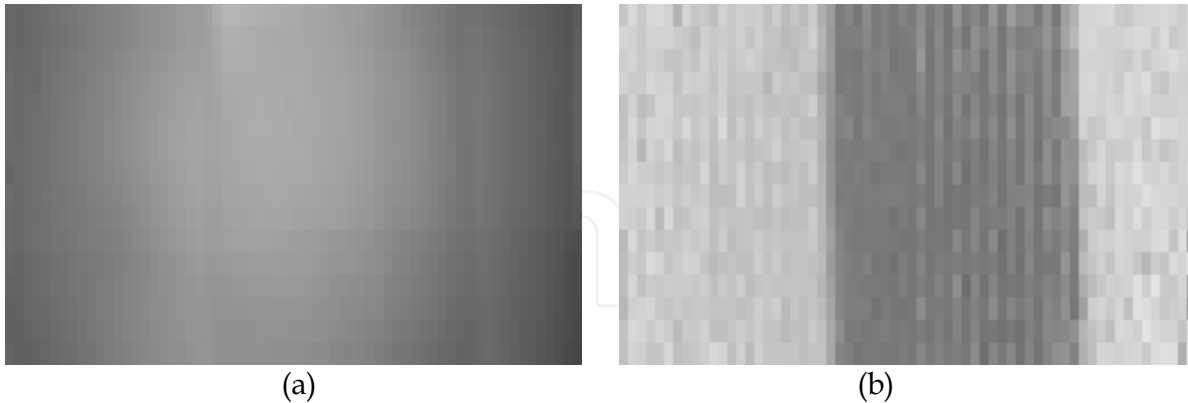


Fig. 3. (a) Gray level value image and (b) TOF range image of two objects with equal gray level values

The images in Fig. 3 are taken with a PhotonICs® PMD 1k-S (64 x 16 Pixel) sensor chip. Fig. 3 (a) shows the gray level values of an object in front of a wall at different distances. Both objects have almost the same gray level values and are very difficult to distinguish. Hence a SV vision system without active lighting, generating shadows, can not estimate the 3D information of the objects due to the correspondence problem. However, a TOF vision system measures the range to the object for each pixel and therefore delivers evenly distributed 3D information as shown in Fig. 3 (b). Hence even a TOF vision system with fewer pixels than a SV vision system can deliver more 3D information when the SV vision system has too many false range matches. This can happen when the captured scenes have too many areas with equal gray level values. The advantage of TOF over a SV vision system is that the TOF ranging technique does not produce incomplete range data (no shadow effects) because illumination and observation directions can be collinear.

3. Design of PMD TOF vision systems

3.1 Range calculation

A PMD TOF sensor generates a range output voltage which can be described as follows (Schwarte & Heinol, 1999):

$$\Delta U_{ab}(T_L) = K \cdot \int_0^{T_{int}} P_{opt}(t - T_L) \cdot u_m(t) dt \quad (3)$$

The range output voltage $\Delta U_{ab}(T_L)$ is determined by the correlation result of the optical echo $P_{opt}(t - T_L)$ and the modulation voltage $u_m(t)$ over the integration time T_{int} . K is a system constant. State of the art is to use CW modulation with square waves. Hence the modulation voltages can be easily generated digitally with a high accuracy and stability using programmable logic devices (PLDs) such as microcontrollers, complex programmable logic devices (CPLD) or field programmable gate arrays (FPGA). The low-pass characteristic of the IR-LEDs leads to an attenuation of the square waves' harmonics for larger frequencies. This results in an optical output that gradually looks sinusoidal for frequencies larger than

5-10 MHz. This has to be taken into account if CW modulation with square waves is used. The modulation voltage $u_m(t)$ and the optical echo $P_{opt}(t-T_L)$ is then given by:

$$u_m(t) = \sum_{n=-\infty}^{\infty} \text{rect}(\omega t - \pi/2 - n \cdot 2\pi) = \frac{4}{\pi} \sum_{k=1}^{\infty} \frac{\sin((2k-1)\omega t)}{(2k-1)} \quad (4)$$

and

$$P_{opt}(t-T_L) = a \cdot (A + \sin(\omega t - \omega T_L)) \quad (5)$$

Equation (4) shows the square wave signal of the modulation voltage $u_m(t)$. Using Fourier series we can write an ideal square wave as an infinite series of only odd integer harmonics. Equation (5) shows the sinusoidal signal echo $P_{opt}(t-T_L)$ of the IR-LEDs. It is assumed that only the fundamental harmonic is transmitted due to the finite bandwidth of the IR-LEDs. The amplitude a of the optical echo $P_{opt}(t-T_L)$ depends on the reflectivity coefficient. In addition the background light is taken into account by adding a constant A . Furthermore it is assumed that a and A are constant during the capture of one range image. Hence $\Delta U_{ab}(T_L)$ will be different for different amplitudes of the optical echo and will cause problems in determining the phase difference between the optical echo $P_{opt}(t-T_L)$ and the modulation signal $u_m(t)$. The amplitude dependency of the output voltage $\Delta U_{ab}(T_L)$ can be avoided by using a phase-shift algorithm. This algorithm is based on the cross correlation of two periodical signals which are shifted in phase to each other. The correlation function $\varphi_{sg}(\tau)$ is defined as follows:

$$\varphi_{sg}(\tau) = s(t) \otimes g(t) = \lim_{T \rightarrow \infty} \frac{1}{T} \int_{-\frac{T}{2}}^{\frac{T}{2}} s(t) \cdot g(t+\tau) dt \quad (6)$$

If we deploy equation (6) to our TOF system $s(t)$ and $g(t+\tau)$ can be written as

$$s(t) = P_{opt}(t-T_L) \quad \text{and} \quad g(t+\tau) = u_m(t+\tau) \quad (7)$$

Then the correlation function $\varphi_{sg}(\tau)$ of the TOF system can be represented as follow:

$$\varphi_{sg}(\tau) = \lim_{T \rightarrow \infty} \frac{1}{T} \int_{-\frac{T}{2}}^{\frac{T}{2}} a \cdot [A + \sin(\omega t - \varphi_0)] \cdot \left[\frac{4}{\pi} \sum_{k=1}^{\infty} \frac{\sin((2k-1)\omega(t+\tau))}{(2k-1)} \right] dt \quad (8)$$

Only the fundamental harmonic of the modulation voltage and the optical echo have the same frequency. Hence the multiplication of these correlated signals results in a DC component and a sinusoidal component with twice the frequency. All other multiplications result in sinusoidal components. After the integration only the DC component remains. Due to this feature of the PMD sensor all other uncorrelated noise sources such as sun light or modulated light sources are suppressed. The DC component is given by:

$$\varphi_{sg}(\tau) = \frac{2 \cdot a}{\pi} \cdot \cos(\varphi_0 + \tau) \quad (9)$$

$\varphi_0 = \omega T_L$ and represents the phase difference between the sent and the received signal. If we now consider equation (9) for example for four different phases $\tau = 0^\circ$, $\tau = 90^\circ$, $\tau = 180^\circ$ and $\tau = 270^\circ$, the correlation result is:

$$\begin{aligned} \varphi_{sg}(0^\circ) &= \frac{2 \cdot a}{\pi} \cdot \cos(\varphi_0), & \varphi_{sg}(90^\circ) &= -\frac{2 \cdot a}{\pi} \cdot \sin(\varphi_0), \\ \varphi_{sg}(180^\circ) &= -\frac{2 \cdot a}{\pi} \cdot \cos(\varphi_0) & \text{and} & \varphi_{sg}(270^\circ) = \frac{2 \cdot a}{\pi} \cdot \sin(\varphi_0) \end{aligned} \tag{10}$$

Now we can calculate the phase difference φ_0 without any dependency on the received optical echo's amplitude a .

$$\varphi_0 = \arctan\left(\frac{\varphi_{sg}(270^\circ) - \varphi_{sg}(90^\circ)}{\varphi_{sg}(0^\circ) - \varphi_{sg}(180^\circ)}\right) \tag{11}$$

Equation (8) is equivalent to equation (3), hence equation (11) can be rewritten as:

$$\varphi_0 = \arctan\left(\frac{\Delta U_{ab}(270^\circ) - \Delta U_{ab}(90^\circ)}{\Delta U_{ab}(0^\circ) - \Delta U_{ab}(180^\circ)}\right) \tag{12}$$

The range value R can now be calculated by taken into account the non-ambiguity range (NAR) at a given modulation frequency of $f_{mod} = 20\text{MHz}$:

$$R = NAR \cdot \frac{\varphi_0}{360^\circ} \tag{13}$$

3.2 Range resolution

The performance and hence the range resolution of solid-state imagers is limited by several different noise sources. Three major noise sources exist: (1) photon shot noise, (2) photocharge conversion noise and (3) quantization noise (Theuwissen, 1995). All of these noise sources can be reduced or eliminated by different signal processing techniques or cooling, except photon shot noise. Hence it is the ultimate theoretical limitation of all photo detectors. Since photon shot noise increases with the amount of incoming photons, it finally dominates all other noise sources and hence limits the effective signal-to-noise ratio for higher illumination levels. Shot noise describes the statistical Poisson-distributed nature of the arrival process of photons and the generation process of electron-hole pairs. The standard deviation of shot noise is equal to the square root of the number of photons (optical shot noise) or photogenerated charge carriers (electronic shot noise). In (Lange, 2000) the required number of photoelectrons per sampling point and pixel to achieve a given range resolution using a 4-phase shift algorithm is derived. It is given by:

$$\Delta R = NAR \cdot \frac{\Delta\varphi_0}{360^\circ} = \frac{c}{4 \cdot \sqrt{8} \cdot f_{mod}} \cdot \sqrt{\frac{B}{M^2}} \tag{14}$$

M is the (de)modulation amplitude, i.e. the number of photoelectrons per pixel and sampling point generated by the modulated light source. M depends on the modulation

depth of the modulated signal and the demodulation contrast of the pixel but also on the optical power of the modulated light source and the target's distance and reflectivity. B is the Offset or acquired optical mean value, i.e. the number of photoelectrons per pixel and sampling point generated by incoming light of the scene's background and the mean value of the received modulated light.

As in practise only the voltage values at the output stages can be measured, equation (14) has to be reformulated. The conversion process of the optically generated charge into an analogous output voltage is characterized using the sensitivity s . The sensitivity is determined by the size of the conversion capacitance C_{int} and the amplification of the output stage A_{os} of the solid-state imager. It is usually specified in terms of volts per electron and is given by Equation (15), where q is the elementary charge ($1.6 \cdot 10^{-19}$ C).

$$s = \frac{A_{os}}{C_{int}} \cdot q \quad (15)$$

Subsequently the output voltage v_{out} of the solid-state imager can be described by Equation (16), where E is the total number of all electrons accumulated in the conversion capacitance. E is the sum of the acquired optical mean value B and the (de)modulation amplitude M .

$$v_{out} = s \cdot E = s \cdot (M + B) \quad (16)$$

Hence the mean value of v_{out} is related to B and the peak-to-peak value of v_{out} is related to M as given in Equation (17).

$$\bar{v}_{out} = s \cdot B \quad \text{and} \quad v_{outPP} = 2 \cdot s \cdot M \quad (17)$$

Now we can rewrite Equation (14) by taken into account equation (17):

$$\Delta R = \frac{c}{2 \cdot \sqrt{8} \cdot f_{mod}} \cdot \sqrt{\frac{\bar{v}_{out}}{v_{outPP}^2} \cdot s} \quad (18)$$

Looking at equation (18) it can be concluded that a large background brightness, which is proportional to \bar{v}_{out} , not only restricts the number of available quantization levels but also drastically increases the quantum noise of the system. Background illumination can be reduced by measuring in the dark or by using spectral filters that only transmit the spectrum of the modulated light. Furthermore it can be concluded that an increasing active modulation power density, which is proportional to v_{outPP} , leads to a better range resolution. As the active optical power density increases with decreasing distance to the object, the ranging accuracy also increases for smaller distances. This is an important fact for navigation applications, where a high accuracy is often only needed close to the target.

Equation (18) can be used to determine the resolution of PMD TOF sensors. The intensity output voltage ΣU_{ab} (see (Schwarte & Heinol, 1999)) of these sensors corresponds to the total number of all electrons accumulated in the conversion capacitance. Hence ΣU_{ab} can be expressed as:

$$\Sigma U_{ab} = s \cdot E = s \cdot (M + B) \quad (19)$$

The modulation amplitude M is related to the absolute value of the range output voltage ΔU_{ab} of the PMD TOF sensor:

$$|\Delta \hat{U}_{ab}| = s \cdot M \quad (20)$$

Hence equation (18) can now be reformulated for the use of a PMD TOF sensor:

$$\Delta R = \frac{c}{4 \cdot \sqrt{8} \cdot f_{\text{mod}}} \cdot \sqrt{\frac{\Sigma U_{ab} - |\Delta \hat{U}_{ab}|}{\Delta \hat{U}_{ab}^2}} \cdot s \quad (21)$$

In (Lange, 2000) it is shown that equation (14) can be expanded to include additional noise sources such as $1/f$ -, reset- and thermal noise by adding an additional number of pseudo-background-electrons N_{pseudo} to B . These noise sources are not correlated to the modulation signal and thus contribute to B rather than M .

$$\Delta R = NAR \cdot \frac{\Delta \varphi_0}{360^\circ} = \frac{c}{4 \cdot \sqrt{8} \cdot f_{\text{mod}}} \cdot \sqrt{\frac{B + N_{\text{pseudo}}}{M^2}} \quad (22)$$

The number of pseudo-electrons N_{pseudo} can be obtained by squaring the noise equivalent number of noise electrons N . These can be determined by measuring v_{dark} and dividing it by the sensitivity s of the sensor.

$$N_{\text{pseudo}} = N^2 = \left(\frac{v_{\text{dark}}}{s} \right)^2 \quad (23)$$

Equation (21) can now be modified to include the additional noise sources. As all electrons generated in the dark should be taken into account the dark voltage is equivalent with the intensity output voltage ΣU_{ab} of the PMF TOF sensor.

$$\Delta R = \frac{c}{4 \cdot \sqrt{8} \cdot f_{\text{mod}}} \cdot \sqrt{\frac{(\Sigma U_{ab} - |\Delta \hat{U}_{ab}|) \cdot s + \Sigma U_{ab \text{dark}}^2}{\Delta \hat{U}_{ab}^2}} \quad (24)$$

If no background light is present and only the active illumination source is active the highest range resolution can be achieved. The modulation amplitude M is then equal to the optical mean value B . Equation (24) can be simplified to:

$$\Delta R = \frac{c}{4 \cdot \sqrt{8} \cdot f_{\text{mod}}} \cdot \sqrt{\frac{s}{|\Delta \hat{U}_{ab}|} + \left(\frac{\Sigma U_{ab \text{dark}}}{\Delta \hat{U}_{ab}} \right)^2} \quad (25)$$

The range accuracy, which can only be improved by averaging, is the absolute limit of a PMD TOF sensor using a 4-phase shift algorithm. The range resolution also depends on the modulation frequency. The higher the modulation frequency the better is the range resolution. However the measuring range (FOV) will decrease with increasing modulation

frequency (see section 2.3). In practice it has shown that increasing the modulation frequency far above 20 MHz will not increase the range resolution because the power of the IR-LEDs will decrease at the same time.

4. Automotive applications using PMD TOF vision systems

4.1 Advantages of PMD TOF vision systems for automotive applications

As mentioned in the introduction section already, TOF vision systems are found in a variety of applications such as industrial sensor systems, automation, robotics, user interfaces, virtual reality and so forth. However the technically most challenging and interesting application is the automotive industry. An appropriate 3D vision system should be able to recognize dangerous situations foresighted to support the driver in the best possible way to avoid accidents. In the case that an accident can not be avoided the system should at least minimize the injury risk for all passengers.

Up to now application-specific sensor units are designed for each particular automotive application. Hence nowadays only pure range measuring systems (long or short range radar, lidar or ultrasonic sensors) or pure opto-electronical 2D camera systems exist in various car assemblies. Increasingly optimized algorithms are developed to fuse the data of different sensor units. This approach is understandable as no system was available to deliver 2D intensity images and range data at the same time. What was missing is a precise, economical, compact, universal sensor technology which can acquire the 3D information (intensity and range information) of a scene in one image capture. Such a technology would deliver the absolute geometrical dimensions of objects without depending on the object surface, - distance, -rotation and -illumination (rotation-, translation- and illumination invariant). SV vision systems were the first to be developed for the automotive industry with the listed disadvantages in section 2. Subsequently the PMD technology was successfully developed which is a TOF vision system with inherent suppression of uncorrelated light signals such as sun light or other modulated light disturbances (Moeller et al., 2005). More advantages of a PMD TOF vision system are the acquisition of the intensity and range data in each pixel without high computational cost and any moving components as well as the monocular setup.

All these advantages lead to a compact and economical design of an automotive 3D TOF vision system. This system can immediately acquire the scene objects parameters without high computational power. The typical frame rate of the system is 100 Hz leading to a high constant 3D data flow. A reliable object plausibility check and calculation of the object motion vectors are possible. Hence a reliable scene interpretation for automotive applications is given. The high frame rate is very important for car safety applications to detect high dynamical changes in the traffic even at a high car speed. With such a system the driver can be best possible supported and the injury risk in a non avoidable collision can be minimized by using active safety measures.

At the moment several automotive manufacturer are using the PMD technology for many different applications such as smart airbag, driver assistant systems, pre crash systems, stop & go systems, pedestrian safety systems, emergency break systems, gesture recognition systems and so force (Ringbeck et al., 2007; Ringbeck & Hagebeuker, 2007; Buxbaum & Hagebeuker, 2005). Fig. 4 and Fig. 5 show some of the realized systems. In the next section a developed PMD TOF vision system usable for pedestrian detection, stop & go and pre crash application is exemplary presented.



Fig. 4. Smart airbag application using a PMD TOF vision systems (Hussmann & Hess, 2006)

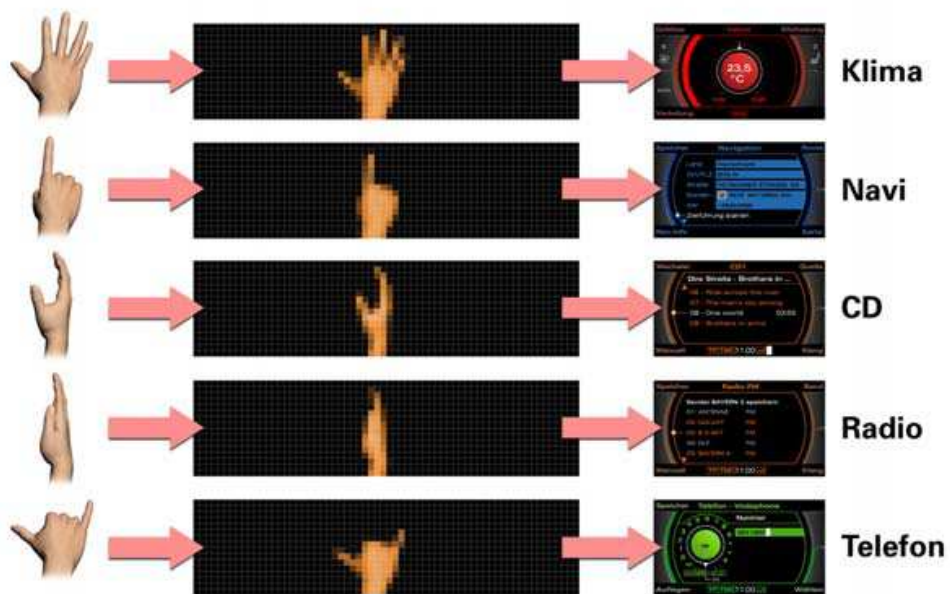


Fig. 5. Gesture recognition using a PMD TOF vision systems (Hussmann & Hess, 2006)

4.2 PMD sensor system for automotive outdoor applications

Fig. 6 shows a PMD sensor system for automotive outdoor applications. This 'A-Muster' camera is designed to demonstrate solutions for several front view applications such as Stop&Go, PreCrash and Pedestrian Safety. The non-ambiguity range (NAR) of the sensor system is 120 m using a modulation frequency of 6,2 and 7,5 MHz. This range is the maximum possible measuring range if enough illumination power is available. To achieve a measuring range as close as possible to the NAR, additional IR-illumination sources can be implemented inside the head lights to increase the transmitted power. For a typical measurement range of 10 m an illumination source with a power rating of 1 W optical power is placed beside the camera system inside the car as shown in Fig. 6 (c). For a measurement range above 35 m a more powerful illumination source has to put into the front of the car as shown in Fig. 6 (b). The range resolution for both measurement ranges is ± 10 cm.

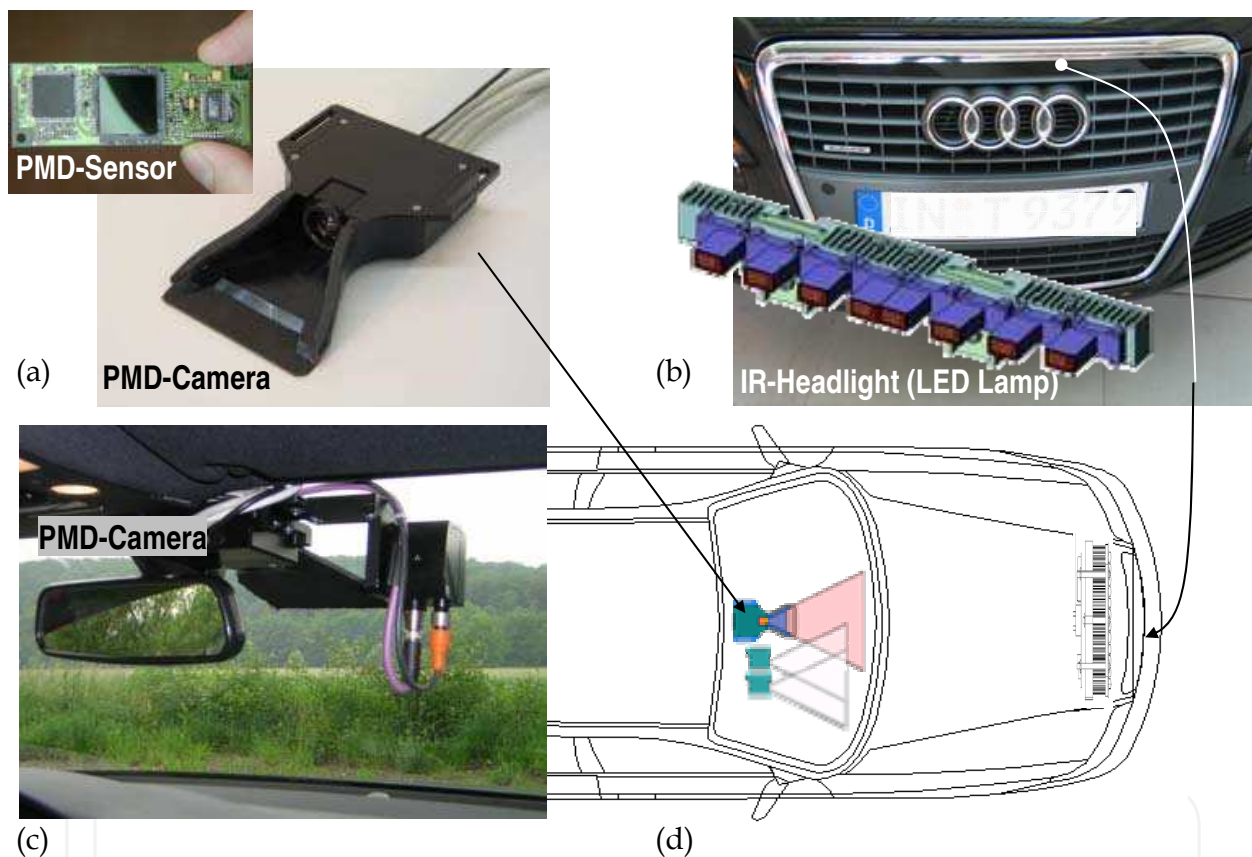


Fig. 6. Illustration of a PMD TOF vision systems for several automotive outdoor applications
 (a) 'A-Muster' PMD camera and PCB with the PhotonICs® PMD 1k-S (64 x 16 Pixel)
 (b) IR-LED Headlights (8 W)
 (c) Internal car setup (PMD camera + 1 W IR-LED illumination source)
 (d) Schematic of overall car setup options

The PMD camera delivers an evenly distributed range image of the observed scene in front of the car. The field of view of the observed scene depends on the chosen optic and the active illumination source and has to be adapted to match the requirements for the implemented outdoor application (Stop&Go, PreCrash and Pedestrian Safety).

Fig. 7 shows the processing chain of the PMD TOF vision system. The pre-processing of the camera's row data is simple and does not require a powerful processing unit. Only the range

and intensity values are calculated as derived in section 3. Furthermore the verification and selection of the feasible range values and the illumination control are processed in this stage. A clear range image is the result of this stage. In the next stage object segmentation and detection algorithm determined the objects in front of the car. The implemented software varies depending on the chosen application. The output of this stage results in an object list. The dynamical objects in the observed scene are tracked in the next stage and a decision is made based on the dynamical objects' position to activate or not activate the actuators. This decision can be confirmed by collected and fused data of other sensor systems.

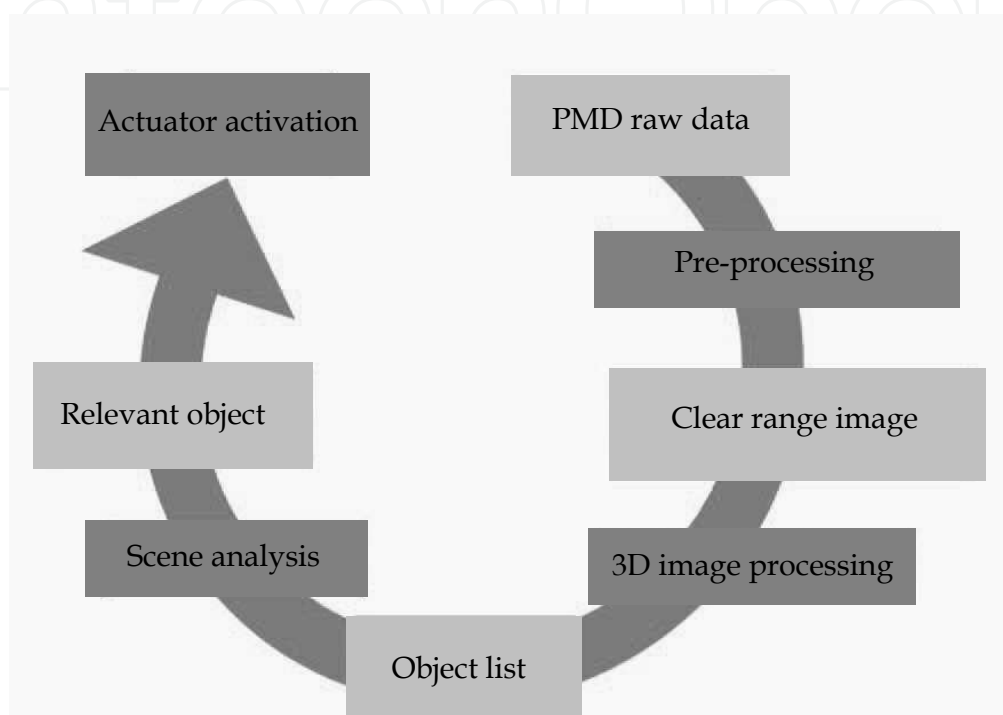


Fig. 7. Processing chain of the PMF TOF vision system

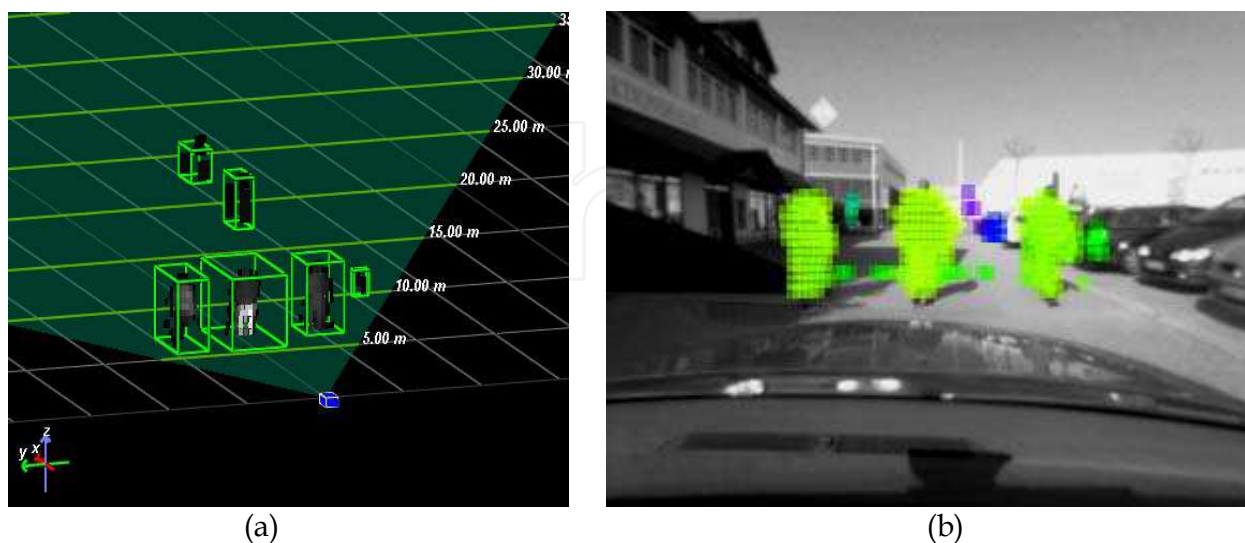


Fig. 8. Experimental results of an observed traffic scene with the PMD TOF vision system
 (a) Range raw data and the resulting object presentations in a virtual 3D space
 (b) Conventional video image with chronological superimposed object visualization

In the following figures the raw data and the resulting object representations of the PMD TOF vision system are depicted at different traffic scenarios. The position of the objects is detected in the 3D space. The position changes are used to determine the motion vectors. Now the objects can be tracked and identified in the observed traffic scenes. This process is illustrated in Fig. 8. Three pedestrians are identified as relevant objects and their position are determined, visualized and tracked.

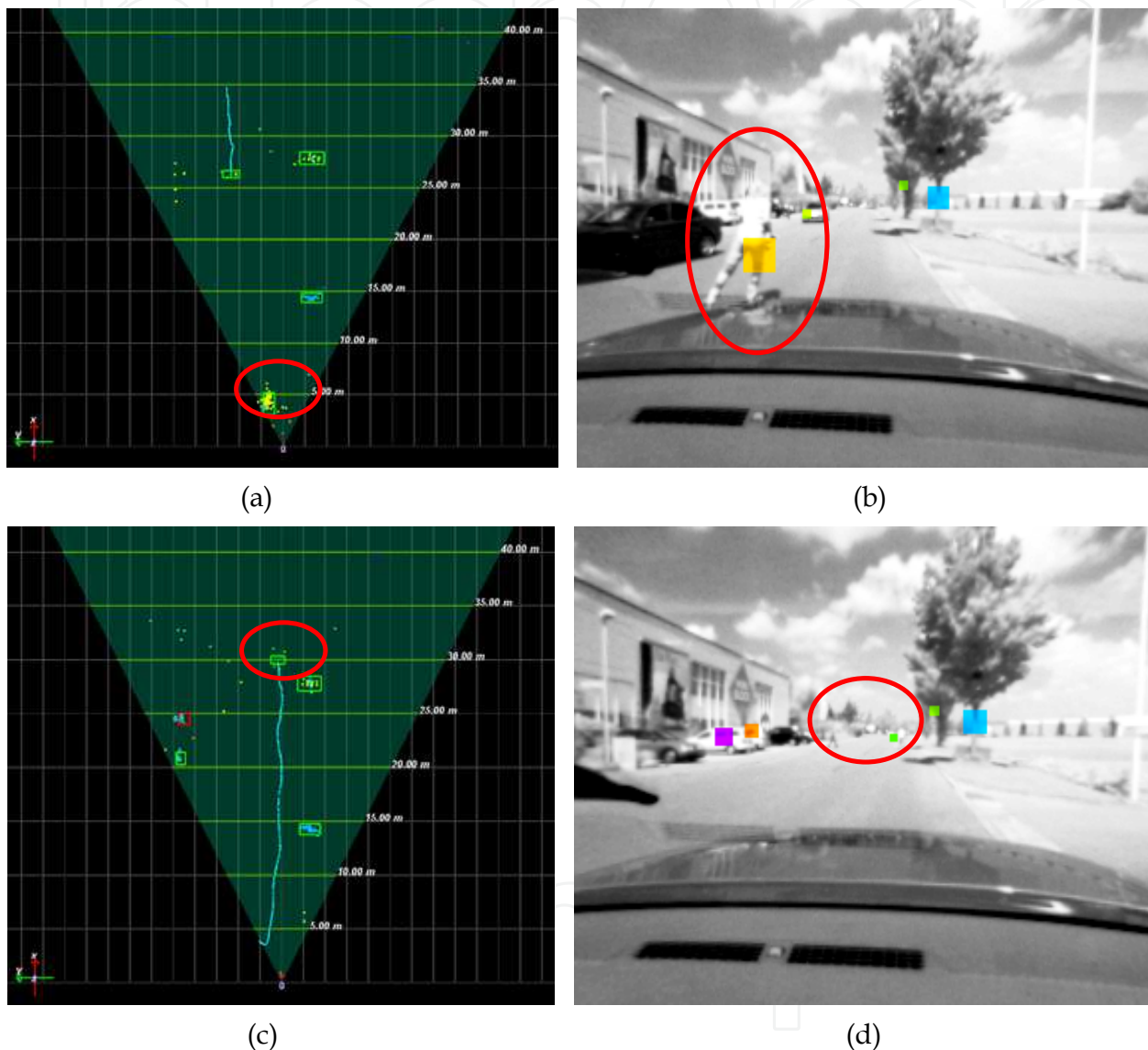


Fig. 9. (a) Range raw data and the resulting object representation of a roller skater (green rectangle in the red circle) after he entered the field of view of the PMD TOF camera
 (b) Conventional video image with chronological superimposed object visualization of the roller skater (yellow rectangle in the red circle)
 (c) Range raw data and the resulting object representation of the roller skater at 30 m (green rectangle in the red circle) as well as the tracked way (blue line)
 (d) Conventional video image with chronological superimposed object visualization of the roller skater (green rectangle in the red circle)

Due to the computational efficient and simple processing chain of the PMD TOF vision system (see Fig. 7), the image processing algorithms are simple and fast. Hence a fast object tracking is possible. Fig. 9 shows a roller skater who is detected and tracked as a relevant object over a range of 30 m. The decision if the roller skater is a relevant object is made straight after he entered the field of view of the PMD TOF camera. This proves the speed of the processing chain of the PMD system.

The tracking of relevant objects is not only possible at low car speeds but also at high car speeds for example on the motorway. Fig. 10 shows the performance of the object tracking on the motorway of the PMD TOF vision system. It has to be noted that the tracking at 50 m is successful even when the objects are represented by only a few pixels as shown in Fig. 10 (b). This accuracy is only possible because every pixel delivers a range value besides its intensity value. This inherent feature of the PMD TOF vision system distinguishes the PMD technology from typical SV vision systems.

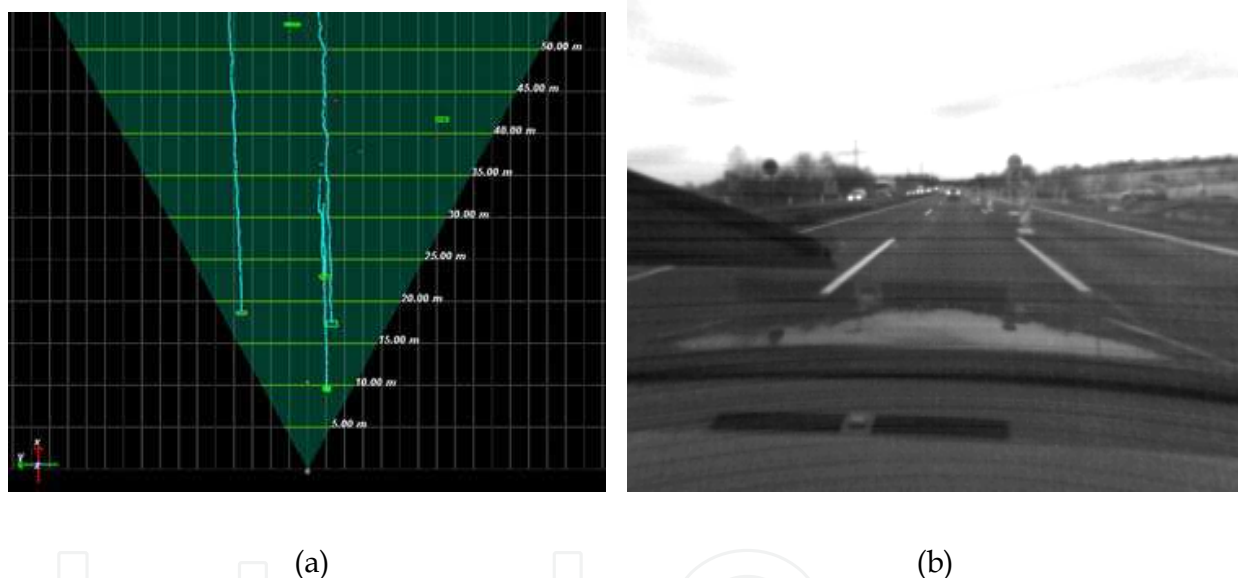


Fig. 10. Object tracking on the motorway using the PMD TOF Vision system
(a) Range raw data and the resulting object representation of cars on the motorway at different ranges (green rectangles) as well as their tracked ways (blue lines)
(b) Conventional chronological video image

5. Conclusion

In this chapter we compared conventional stereo vision systems with time-of-flight vision system and highlighted the advantages and disadvantages of both systems. The new PMD technology represents a TOF vision system with many advantages in comparison to conventional stereo vision systems especially in the automotive industry. The equations needed for the design of such a system are derived and demonstrate the simplicity of the

extraction of the range information. A PMD camera delivers absolute geometrical dimensions of objects without depending on the object surface, - distance, -rotation and - illumination. Hence PMD TOF vision systems are rotation-, translation- and illumination invariant.

The major advantage of the PMD technology is the delivery of an evenly distributed range and intensity images because each pixel calculates a range and intensity value. Hence the correspondence problem of conventional stereo vision system does not exist. Another advantage of the PMD technology is that the field-of-view can easily be extended by varying the modulation frequency without any special optical components. However, the range resolution depends on the chosen modulation frequency. The higher the modulation frequency the better the resolution and the smaller the measuring range. The range resolution depends also on the power rating of the used active illumination source. Furthermore it has been shown that the range data of the 3D-TOF camera is almost independent on the reflection coefficient of the measured objects if a phase-shift algorithm is used. The PMD technology has an inherent suppression of uncorrelated light signals such as sun light or other modulated light disturbances. However if those light sources saturate the sensor, the range information is lost. More advantages of a PMD technology are the acquisition of the intensity and range data in each pixel without high computational cost and any moving components as well as the monocular setup.

All these advantages lead to a compact and economical design of an automotive 3D TOF vision system with a high frame rate. This vision system can be used for many different applications such as smart airbag, driver assistant systems, pre crash systems, stop & go systems, pedestrian safety systems, emergency break systems, gesture recognition systems and so forth. In this chapter experimental results of a PMD TOF vision system for automotive outdoor applications such as Stop&Go, PreCrash and Pedestrian Safety are presented and demonstrate that the accuracy of the system is appropriate to fulfil the tough target settings in the automotive industry.

6. References

- Beheim, G. & Fritsch, K. (1986). Range finding using frequency-modulated laser diode, *Applied Optics*, 25 (9), pp. 1439-42
- Benosman, R., Maniere, T. & Devars, J. (1996). Multidirectional stereovision sensor, calibration and scene reconstruction, *IEEE Int. Conf. on Pattern Recognition, ICPR*, vol.1, pp. 161-5
- Buxbaum, B. & Hagebeuker, B. (2005). Dreidimensionale Umfeld-Erfassung, *Trade Journal: "Elektronik automotive"*, WEKA Publisher House, Issue 5, ISSN 1614-0125, pp. 77-81
- Cheng, S., Tu, D., Li, G. & Yang, J. (2002). Fusing Range and 2-D images in multisensor for robot vision, *IEEE TENCON*, pp. 565-568
- Dhond, U.R. & Aggarwal, J.K. (1989). Structure from stereo - A review, *IEEE Trans. On Systems, Man and Cybernetics*, 19 (6), pp. 1489-1508
- Hess, H., Albrecht, M., Grothof, M., Hussmann, S., Oikonomidis, N. & Schwarte, R. (2003). 3D object recognition in TOF data sets, *Proc. SPIE*, vol. 5086, pp. 221-228

- Hussmann, S. & Hess, H. (2006). Dreidimensionale Umwelterfassung, *Trade Journal: "Elektronik automotive"*, WEKA Publisher House, Issue 8, ISSN 1614-0125, pp. 55-59
- Hussmann, S. & Liepert, T. (2007). Robot Vision System based on a 3D-TOF Camera, *IMTC 2007, IEEE Proc. of the 24th Int. Conf. on Inst. and Meas. Tec.*, pp. 1-5
- Kang, S.B. & Szeliski, R. (1997). 3-D scene data recovery using omnidirectional multibaseline stereo, *International Journal of Computer Vision*, 25 (2), pp. 167-83
- Kawanishi, T., Yamazawa, K., Iwasa, H., Takemura, H., & Yokoya, N. (1998). Generation of high resolution stereo panoramic images by omnidirectional imaging sensor using hexagonal pyramidal mirrors, *Int. Conf. on Pattern Recognition, ICPR*, pp. 485-489
- Krishnan, A. & Ahuja, N. (1996). Range estimation from focus using a non-frontal imaging camera, *International Journal of Computer Vision*, 20 (3), pp. 169-185
- Lange, R. (2000). 3D Time-of-flight distance measurement with custom solid-state image sensors in CMOS/CCD-technology, *PhD thesis*, Dep. of Electrical Engineering and Computer Science, University of Siegen, Online publication: <http://www.ub.uni-siegen.de/epub/diss/lange.htm>
- Liancheng, S. & Feng Z. (2005). Design of a novel stereo vision navigation system for mobile robots, *IEEE Int. Conf. on Robotics and Biomimetics (ROBIO)*, pp. 611-614
- Lin, S.S. & Bajcsy, R. (2003). High resolution catadioptric omni-directional stereo sensor for robot vision, *Int. Conf. On Robotics & Automation*, pp. 1694-1699
- Moeller T., Kraft H., Frey J., Albrecht M. & Lange R. (2005). Robust 3D Measurement with PMD Sensors, *RIM-Day*, ETH Zürich, Online-publication (<http://www.pmdtec.com/inhalt/download/documents/RIM2005-PMDTec-Robust3DMeasurements.pdf>)
- Moring, I., Heikkinen, T., Myllyla, R. & Kilpela, A. (1989). Acquisition of three-dimensional image data by a scanning laser range finder, *Optical Engineering*, 28 (8), pp. 897-902
- Ringbeck, T. & Hagebeuker, B. (2007). A 3D Time of flight camera for object detection, *Optical 3-D Measurement Techniques*, ETH Zürich, Online-publication (<http://www.pmdtec.com/inhalt/download/documents/070513Paper-PMD.pdf>)
- Ringbeck, T., Hagebeuker, B., Kraft, H. & Paintner, M. (2007). PMD-basierte 3D-Optosensoren zur Fahrzeugumfelderfassung, In: *Sensoren im Automobil II*, Thomas Tille, pp. 209-222, Expert Verlag GmbH, ISBN: 3816927505
- Schwarte_a, R., Xu, Z., Heinol, H., Olk, J. & Buxbaum, B. (1997). New optical four-quadrant phase-detector integrated into a photogate array for small and precise 3D-cameras, *Proc. SPIE*, vol. 3023, pp. 119-128
- Schwarte_b, R., Xu, Z., Heinol, H., Olk, J., Klein, R., Buxbaum, B., Fischer, H. & Schulte, J. (1997). New electro-optical mixing and correlating sensor: facilities and applications of the photonic mixer device (PMD), *Proc. SPIE*, vol.3100, pp. 245-53

- Schwarte, R. & Heinol, HG. (1999). Optical component combines 3D image detection and mixing, *Elektronik*, Publisher: WEKA-Fachzeitschriften, Germany, 48(12), pp. 80-90
- Theuwissen, A. (1995). Solid-State Imaging with Charge-Coupled Devices, *Kluwer Academic Publishers*, ISBN-13: 978-0792334569

IntechOpen

IntechOpen



Stereo Vision

Edited by Asim Bhatti

ISBN 978-953-7619-22-0

Hard cover, 372 pages

Publisher InTech

Published online 01, November, 2008

Published in print edition November, 2008

The book comprehensively covers almost all aspects of stereo vision. In addition reader can find topics from defining knowledge gaps to the state of the art algorithms as well as current application trends of stereo vision to the development of intelligent hardware modules and smart cameras. It would not be an exaggeration if this book is considered to be one of the most comprehensive books published in reference to the current research in the field of stereo vision. Research topics covered in this book makes it equally essential and important for students and early career researchers as well as senior academics linked with computer vision.

How to reference

In order to correctly reference this scholarly work, feel free to copy and paste the following:

Stephan Hussmann, Thorsten Ringbeck and Bianca Hagebeuker (2008). A Performance Review of 3D TOF Vision Systems in Comparison to Stereo Vision Systems, Stereo Vision, Asim Bhatti (Ed.), ISBN: 978-953-7619-22-0, InTech, Available from:

http://www.intechopen.com/books/stereo_vision/a_performance_review_of_3d_tof_vision_systems_in_comparison_to_stereo_vision_systems

INTECH

open science | open minds

InTech Europe

University Campus STeP Ri
Slavka Krautzeka 83/A
51000 Rijeka, Croatia
Phone: +385 (51) 770 447
Fax: +385 (51) 686 166
www.intechopen.com

InTech China

Unit 405, Office Block, Hotel Equatorial Shanghai
No.65, Yan An Road (West), Shanghai, 200040, China
中国上海市延安西路65号上海国际贵都大饭店办公楼405单元
Phone: +86-21-62489820
Fax: +86-21-62489821

© 2008 The Author(s). Licensee IntechOpen. This chapter is distributed under the terms of the [Creative Commons Attribution-NonCommercial-ShareAlike-3.0 License](#), which permits use, distribution and reproduction for non-commercial purposes, provided the original is properly cited and derivative works building on this content are distributed under the same license.

IntechOpen

IntechOpen